Equilibrium Adsorption in Cylindrical Mesopores: A Modified Broekhoff and de Boer Theory versus Density Functional Theory

E. A. Ustinov,[†] D. D. Do,[*,‡] and M. Jaroniec[§]

Saint Petersburg State Technological Institute (Technical University), 26, Moskovsky Prospect, 190013, Russia, Department of Chemical Engineering, University of Queensland, St. Lucia, Qld 4072, Australia, and Department of Chemistry, Kent State University, Kent, Ohio 44242, U.S.A.

Received: August 2, 2004; In Final Form: November 22, 2004

This paper presents a thermodynamic analysis of capillary condensation phenomena in cylindrical pores. Here, we modified the Broekhoff and de Boer (BdB) model for cylindrical pores accounting for the effect of the pore radius on the potential exerted by the pore walls. The new approach incorporates the recently published standard nitrogen and argon adsorption isotherm on nonporous silica LiChrospher Si-1000. The developed model is tested against the nonlocal density functional theory (NLDFT), and the criterion for this comparison is the condensation/evaporation pressure versus the pore diameter. The quantitative agreement between the NLDFT and the refined version of the BdB theory is ascertained for pores larger than 2 nm. The modified BdB theory was applied to the experimental adsorption branch of adsorption isotherms of a number of MCM-41 samples to determine their pore size distributions (PSDs). It was found that the PSDs determined with the new BdB approach coincide with those determined with the NLDFT (also using the experimental adsorption branch). As opposed to the NLDFT, the modified BdB theory is very simple in its utilization and therefore can be used as a convenient tool to obtain PSDs of all mesoporous solids from the analysis of the adsorption branch of adsorption isotherms of any subcritical fluids.

1. Introduction

Investigations of the capillary condensation and evaporation phenomena have a long history dating back to the early work of Zsigmondy.[1] The simplest approaches were based on the Kelvin equation,[2−5] and this equation has been widely applied in the analysis of pores in the mesopore range. It is now known that this equation fails to quantitatively describe the capillary effects for pores below 10 nm in diameter. Attempts to improve this equation by correcting the meniscus radius accounting for the adsorbed layer thickness were made by Foster,[6] Cohan,[7] and Derjaguin.[8] Barret, Joyner, and Halenda (BJH) utilized the Cohan equations in their method of pore size analysis.[9] The discovery of ordered mesoporous adsorbents such as MCM-41 has shown that the BJH method underestimates pore diameters. A substantial improvement of the Kelvin−Cohan (KC) equations has been done recently by Kruk, Jaroniec, and Sayary (KJS) by introducing a correction for the pore radius.[10−12] In the framework of classical models, the most rigorous thermodynamic analysis of the capillary condensation phenomena in cylindrical pores was first developed by Broekhoff and de Boer (BdB).[13,14] They proceeded from the following simplifying assumptions: (i) the adsorbed phase has the form of a liquid film whose density is equal to that of saturated bulk liquid; (ii) the contribution of a gaslike phase to the amount adsorbed is neglected; (iii) the surface tension of the liquid film is the same as that for the macroscopic liquid and does not depend on the film thickness and the interface curvature; (iv) the dependence of the potential exerted by the solid inside the pore on the distance from its surface is the same as that for the reference nonporous solid of the same chemical structure. This is a critical assumption, as the surface of a pore is not necessary the same as that of a nonporous solid. Despite these simplifications, the BdB model has still remained the most elegant and thermodynamically self-consistent theory for nearly four decades. It can be easily shown that the KC equations are the special case of the BdB theory if the solid−fluid potential inside the pore (at least in the region that encompasses the liquid−vapor interface) is zero. However, in the absence of the external field, the cylindrical meniscus loses its mechanical stability, which makes its existence impossible. As a matter of fact, the grand thermodynamic potential corresponding to the Cohan equation is always maximal, while the thermodynamic equilibrium requires the thermodynamic potential to be minimal. Nevertheless, despite the thermodynamic inconsistency, the BJH method of pore size distribution analysis based on the KC equations enjoys widespread popularity, which may be explained not only by its simplicity but also a belated comparison with molecular approaches.

The BdB theory is a subject of constant investigations in an attempt to improve its applicability against experimental data. For example, Lukens et al.[15] replaced the BdB *t*-curve by the Hill's approximation, which allowed them to obtain simpler equations than those presented in the original paper. More fundamental improvement has been done by Zhu et al.[16] and Qiao et al.[17,18] The authors accounted for the change of the potential exerted by the cylindrical pore wall with the pore diameter, but they did it in an empirical manner, which does not provide universality of their approach. Further development of the BdB theory made by Sonwane and Bhatia (SB)[19−23] was based on incorporation of the surface tension dependence on the interfacial surface curvature. In these works, the effect of

* Corresponding author.
† On leave from Saint Petersburg State Technological Institute (Technical University).
‡ University of Queensland.
§ Kent State University.

10.1021/jp046534u CCC: $30.25
Published on Web 01/15/2005

the solid surface curvature on the solid−fluid potential was also accounted for by the use of the Lennard Jones (LJ) 12-6 pair potential for the interaction between the solid atom and fluid molecule. In general, these improvements exhaust the possibilities of classical approaches. However, all versions of the BdB theory fail to explain experimentally observed peculiarities of the hysteresis phenomena. Thus, in the case of nitrogen adsorption at its boiling point, the hysteresis never exists at the relative pressure less than about 0.42, which corresponds to the critical cylindrical pore diameter of 4 nm.[24] The original BdB theory does not lead to reversibility at all, while Sonwane and Bhatia reported the value of 1.9 nm for the critical pore size,[20] which is, however, substantially smaller than the experimental value of 4 nm. Inoue et al.[25] made an attempt to explain this discrepancy by the so-called intrinsic pore size distribution. They found that if the variance of this distribution is 0.1 nm, which is expected for silica surface, the critical pore diameter increases to 3.6−3.8 nm. It should be noted, however, that this estimation is not correct because of the incorrect application of the BdB theory for the criterion of evaporation. The authors considered the capillary evaporation identically to the vaporlike spinodal condensation, only multiplying the surface tension by 2 (semispherical meniscus), whereas the evaporation pressure corresponds to the equality of grand thermodynamic potential for the completely filled pore and that for the partly filled pore. The similar incorrectness (i.e., the condition that the second derivative of the grand thermodynamic potential with respect to the film thickness is zero for the evaporation pressure) is related to the SB approach.

At present, no theory predicts the hysteresis critical pressure, which is much larger than could be expected and seems to attribute to the physical properties of the fluid, rather than to the solid−fluid system. To explain this phenomenon, the tensile strength hypothesis[26,27] is often resorted to. It is implied that intermolecular bonds in the liquid filling the pore channel break if the hydrostatic pressure inside this channel approaches the critical (negative) value according to the Young−Laplace equation for the hemispherical meniscus. If it is assumed that in the pore center the solid−fluid potential is negligibly small, the hydrostatic pressure will be a single-valued function of the bulk pressure no matter what the pore diameter is, which does explain the existence of the critical bulk pressure and the increase of steepness of the desorption branch in the proximity of the lower closure point of the hysteresis loop. The tensile strength hypothesis is exploited in a number of works[19,21,23,28,29] but still does not have any support from molecular approaches. Anyway, the desorption branch of the isotherm seems to be nonequilibrium. This was recently established by Morishige et al.[30,31] using the temperature dependence of the chemical potential of different fluids adsorbed in MCM-41 and SBA-15 at the condensation and evaporation pressures. It was shown that the curve for desorption has a kink at the hysteresis critical pressure, while the curve for adsorption is a straight line. This has led the authors to the conclusion that the adsorption branch of the isotherm is quite close to the true equilibrium by reasons which are still not quite clear, because theoretically, one should expect that the capillary evaporation rather than condensation is at equilibrium.

For the past decades, the hysteresis phenomena have been intensively investigated by means of the density functional theory (DFT)[32−38] and Monte Carlo simulations.[38−41] Interestingly, although much more rigorous compared to classical theories, these molecular approaches did not provide much more new physical insight, and so, all above-mentioned problems are still unresolved. To some extent, this is expected, because both classical theories and molecular approaches were applied to mesoporous adsorbents, which are not purely microscopical systems. On the other hand, it was shown that quantitative agreement between the BdB theory and the DFT analysis is observed only for pores larger than 7 nm.[34] This suggests that the original BdB theory has an inherent shortcoming, and yet, it could be easily eliminated in the framework of the classical consideration. From our viewpoint, this general shortcoming is the assumption that the potential in the pore is not affected by the curvature of the pore wall and changes with the distance in just the same way as in the case of a flat nonporous reference solid. As we already mentioned, there were some attempts to incorporate the curvature-dependent solid−fluid potential to the BdB model in an empirical manner,[16−18] which, to some extent, causes its devaluation. Another way of improvement was based on a combination of the continuum BdB theory and the LJ solid−fluid pair potential.[19,20] Such a hybridization of the molecular and macroscopic approaches involves a number of additional molecular parameters, making the method less universal and too complex for routine practical applications.

There are three goals of the present paper. The first one is to incorporate into the BdB theory a method of recalculation of the potential exerted by the flat reference surface to the potential inside the cylindrical pore in the framework of purely continuum representation without invoking any molecular parameters such as collision diameters and potential well depth for solid−fluid and fluid−fluid interactions. For this new approach, we coin the term Curvature Dependent Potential−Broekhoff−de Boer (CDP−BdB) theory. The second goal is to compare the CDP−BdB with the original BdB theory and also with the NLDFT for nitrogen adsorption in cylindrical pores having amorphous silica-like walls. To this end, we will show how the conventional DFT could be adapted to the case of fluid adsorption on amorphous surfaces providing highly accurate quantitative description of adsorption isotherms on the reference nonporous silica and in porous materials without artificial layering, which is always observed in the case of the conventional NLDFT. The third goal is the comparative pore size distribution (PSD) analysis of a number of MCM-41 samples by means of the NLDFT, CDP−BdB, and original BdB theories.

2. Model

2.1. A Renewed Version of the Broekhoff and de Boer Theory. We will follow the original model of Broekhoff and de Boer, but relax the assumption "the potential in the pore at a distance t from the pore wall is the same as that nearby the flat surface at the same distance". Our theory retains the essential points of the BdB method including the assumption of constant surface tension, but by accounting for the effect of surface curvature on the potential, we will be able to address smaller pores, of which the analysis is not proper with the original BdB theory. To make all derivations in a coherent manner, we will not use the empirical function of the film thickness defined by Broekhoff and de Boer as the difference between the chemical potential of the saturated liquid and the chemical potential of the adsorbed fluid, which is a bit abstract. Instead, we will use the simplified physical image that the adsorbed phase is modeled as a liquid film bounded by two free surfaces. In the general case, the surface areas of these boundaries are different. We denote S_c as the surface area in contact with the solid and S_t as the surface area of the liquid−vapor interface. If it is assumed that the intrinsic thermodynamic properties of the adsorbed liquid film are the same as those for the bulk liquid in

equilibrium with its vapor, the Helmholtz free energy of the adsorbed film, F, can be expressed as the sum of three terms: (a) the Helmholtz free energy of the free liquid having the same number of moles as that of the adsorbed film, (b) the change in the Helmholtz free energy because of the formation of two free surfaces bounding the adsorbed film, and (c) the potential energy u of interaction between the solid and the molecules in the adsorbed film. The Helmholtz free energy of the free liquid can be obtained by applying the basic thermodynamic relation, $F_L = G_L - pV_L$, where G_L is the Gibbs free energy of the liquid and V_L is the liquid volume occupied by n moles. Thus, the molar Helmholtz free energy of liquid is $\bar{F}_L = \bar{G}_L - p\upsilon_M$, where the upper bar denotes the molar quantity and υ_M is the liquid molar volume. The second term in the right-hand side (RHS) of this equation is usually neglected because of the small value of the liquid molar volume. The molar Gibbs free energy of liquid is taken to be the chemical potential at the saturation pressure (i.e., we neglect the compressibility of liquid). Thus

$$\bar{F}_L \approx \mu^\circ(T) + RT \ln p_0 \tag{1}$$

$$F_L = n\bar{F}_L \tag{2}$$

$$n = \rho_L \int_0^t S(t')\, dt' \tag{3}$$

Here, $\mu^\circ(T)$ is the standard value of the chemical potential, p_0 is the saturation pressure, n is number of moles in the film, ρ_L is the liquid density, t is the film thickness, T is the temperature, and R is the gas constant. The film thickness is defined in a statistically macroscopic sense that is if S is the surface area of a flat surface then $St\rho_L$ is the number of moles in the adsorbed phase. In the case of a cylindrical pore having a radius r and length L, the number of moles in the adsorbed phase is $\pi t(2r - t)L\rho_L$. It is implied that the vapor phase behaves as an ideal gas (this is satisfied by all adsorbates at temperatures commonly used in pore characterization). The second contribution to the Helmholtz free energy of the adsorbed film comes from the fact that some energy is required to form the two interfaces adjacent to the adsorbed film. This is equal to the product of the surface tension and the area of the interfaces, because the surface tension is assumed to be independent of the film thickness and the interface curvature. Hence, we write the following equation for this contribution:

$$F_\Omega = \gamma_c S_c + \gamma S_t \tag{4}$$

Here, S_t and S_c are the area of the internal and external surfaces adjacent to the adsorbed liquid film, respectively, γ and γ_c are the surface tension for the liquid−vapor and solid−liquid interfaces, respectively. In the general case, γ and γ_c are different; yet, the latter disappears in the subsequent derivations, so this difference does not affect the final results.

The third contribution is due to the solid−fluid potential. It is given by

$$F_U = \rho_L \int_0^t S(t')u(t')\, dt' \tag{5}$$

where $u(t')$ is the potential between the solid and one mole of adsorbate at a distance t' from the surface. Thus, we now write the total Helmholtz free energy of the adsorbed film as follows:

$$F = \rho_L[\mu^\circ(T) + RT \ln p_0] \int_0^t S(t')\, dt' + \gamma_c S_c + \gamma S_t + \rho_L \int_0^t S(t')u(t')\, dt' \tag{6}$$

The grand thermodynamic potential is defined as

$$\Omega = F - n\mu \tag{7}$$

Because the vapor phase is assumed to behave as an ideal gas, we can write the chemical potential as follows:

$$\mu = \mu^\circ(T) + RT \ln p \tag{8}$$

Given the Helmholtz free energy in eq 6 and the chemical potential as a function of pressure in eq 8, the thermodynamic grand potential of the adsorbed film can be written in the following explicit form:

$$\Omega = -\rho_L RT \ln(p/p_0) \int_0^t S(t')\, dt' + \gamma_c S_c + \gamma S_t + \rho_L \int_0^t S(t')u(t')\, dt' \tag{9}$$

Given the above expression for the grand potential of the adsorbed film, its equilibrium state can be found by minimizing the grand potential with respect to the adsorbed quantity. The minimum Ω corresponds to the condition $\partial\Omega/\partial n = 0$, which is equivalent to the condition $\partial\Omega/\partial t = 0$. It leads to the following result:

$$\frac{\partial\Omega}{\partial t} = -\rho_L S_t RT \ln(p/p_0) + \gamma \frac{dS_t}{dt} + \rho_L S_t u(t) = 0$$

or, after simplification

$$RT \ln(p/p_0) = \gamma \upsilon_M \frac{d \ln S_t}{dt} + u(t) = 0 \tag{10}$$

Equation 10 allows us to relate the thickness of the adsorbed film as a function of pressure (i.e., isotherm). Knowing $t(p)$, we can readily calculate the grand thermodynamic potential as given in eq 9. This functional dependence of t on p is valid if the grand thermodynamic potential is less than the grand potentials of any other adsorbed phase configurations.

2.1.1. t-Curve and Potential Exerted by the Reference Flat Surface. Broekhoff and de Boer used the experimental data of Cranston and Inkley[42] obtained in 1957 for nitrogen adsorption at 77 K on open surfaces of many mineral powders. The range of relative pressures p/p_0's presented by these authors was from 0.08 to 0.98. A much wider range of pressure for the standard reduced isotherm was recently available for nitrogen adsorption at 77 K[43] and argon adsorption at 77 K[44] and 87.3 K[12] on amorphous silica LiChrospher Si-1000. For example, the pressure range in the case of N_2 adsorption spans over 6 decades, with relative pressures as low as 5×10^{-7}. This set of data will be used in our analysis. The multiplier to convert the standard reduced adsorption data to the t-curve was found from the comparative plot of the amount adsorbed in the primary pore volume of MCM-41 samples versus the amount adsorbed on nonporous silica in the low-pressure region (before the onset of the capillary condensation).[43] This plot is represented by a straight line, suggesting that the film thickness in this pressure region does not depend on surface curvature. Because the pore diameter of an MCM-41 sample was determined independently from XRD analysis and the pore volume is known from the adsorption isotherm (after the external adsorption has been properly accounted for), the statistical film thickness of nitrogen adsorbed in the pore could be calculated. Therefore, it was possible to estimate the surface area of the reference nonporous silica and then plot the t-curve in the entire pressure range. By such a way, a value of 19.65 m^2/g was determined. In the present

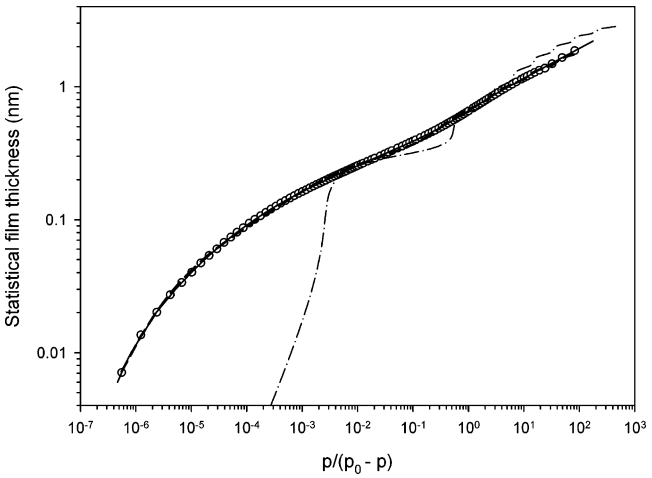

Figure 1. Statistical film thickness vs relative pressure (*t*-curve) for N_2 adsorption on nonporous silica LiChrospher Si-1000 at 77.3 K.[43] Experimental data and the correlation curve are shown by circles and solid line, respectively. Dashed line (merged with solid line) is plotted with the new version of NLDFT. Dash−dotted line is plotted with the conventional NLDFT for the molecular parameters reported in ref 53. The abscissa expresses the value $p/(p_0 - p)$ to show the isotherm more clearly in the pressure region close to the saturation pressure. At low pressure, the abscissa $p/(p_0 - p)$ tends toward the relative pressure p/p_0.

paper, we took the value of 24 m^2/g for the surface area for NLDFT analysis by reasons discussed below. The *t*-curve for nitrogen adsorption on LiChrospher Si-1000 at 77.3 K is presented in Figure 1 for the surface area of 24 m^2/g, where we plot the statistical film thickness t versus $p/(p_0 - p)$ on a logarithmic scale. The choice of the axis $p/(p_0 - p)$ is of benefit in two ways. First, the low-pressure region is enlarged because of the logarithmic scale, while the pressure region near the saturated vapor pressure is enlarged because of the larger value of $p/(p_0 - p)$. Thus, this choice is suitable for presenting the adsorption isotherm over a complete range of pressure from very low to that close to the saturated vapor pressure for subcritical fluids. Interestingly, the *t*-curve in the region of high values of $p/(p_0 - p)$ is approximated by a straight line, a feature that is observed for many other *t*-curves. This interesting feature can be taken advantage of to determine the behavior of the *t*-curve in the region of pressures very close to the saturation pressure. Because the *t*-curve versus $p/(p_0 - p)$ is quite smooth, we can correlate it with a simple mathematical function. For example, this isotherm for the reference adsorbent may be reliably approximated by the power series of the order 4. In the present paper, we rely on the curve-fitting with cubic spline approach. The solid line in the figure is plotted for parameters found by the least-squares technique.

Because for the flat solid surface, the surface area S_t of the liquid film boundary is constant, from eq 10 we obtain the following equation for the solid−fluid potential at the liquid film boundary (i.e., at the distance t from the solid surface)

$$u(t, \infty) = RT \ln(p/p_0) \tag{11}$$

Here, the symbol ∞ denotes the infinite radius of the solid surface curvature, which is valid for the flat surface. Knowing the amount adsorbed and the surface area, we can calculate the statistical film thickness, and because $u(t, \infty)$ is calculated from eq 11, we thence obtain the functional dependence of u on t for a flat reference surface. But, knowing this $u(t, \infty)$ for a flat surface, we need to find a means to obtain the solid−fluid potential $u(t, r)$ for a pore of radius r. This can be done by an introduction of a so-called pairwise potential $\varphi(r)$, which will be discussed in detail in the next section.

2.1.2. Evaluation of the Pair Potential from the t-Curve. We let $\varphi(r)$ be the pair potential energy between one molecule of adsorbate and one solid atom at a distance r. Let us now address how this potential can be obtained experimentally. If the solid is assumed to be a continuum with ρ_s being the number solid density, the solid−fluid potential is then simply obtained from the following integral

$$u(t, \infty) = N_A \rho_s \int_t^\infty \varphi(r) S(r)\, dr \tag{12}$$

where N_A is Avogadro's number, and $S(r) = 2\pi r(r - t)$ is the area of the spherical segment overlapped by a sphere having a radius r and the solid. Differentiating of the solid−fluid potential of eq 12 twice with respect to t leads to the following explicit equation for the pairwise potential $\varphi(r)$:

$$\varphi(r) = \frac{1}{2\pi N_A \rho_s} \left(t^{-1} \frac{d^2 u(t, \infty)}{dt^2} \right)_{t=r} \tag{13}$$

This equation will form a basis to determine the intrinsic pairwise interaction energy $\varphi(t)$ if we know the experimental data of a reference flat surface. Having the data, we can determine the potential u from eq 11 as a function of t, from which the pairwise solid−fluid potential can be computed from the above equation.

2.1.3. Determination of the Potential in the Cylindrical Pore from the t-Curve. Once we know the pairwise potential energy, the solid−fluid potential for any other geometry can be readily determined, as we will show for the case of a cylindrical pore of infinite extent. The potential of one mole of adsorbate $u(t, r)$ (where r is the pore radius) at the distance t from the cylindrical surface is given by

$$u(t, r) = N_A \rho_s \int_t^\infty \varphi(r') S(t, r, r')\, dr' \tag{14}$$

where r is the pore radius and $S(t, r, r')$ is the area of the spherical segment of radius r' with the center at the distance t from the pore wall, which is completely found in the solid surrounding the cylindrical pore of radius r

$$S(t, r, r') = 4r'^2 \int_0^\vartheta \cos\alpha\, d\vartheta \tag{15}$$

where α is the angle between the vector $\mathbf{r}'$ and the pore axis, and ϑ is the radial angle. The upper limit of the above integral is given by

$$\vartheta = \begin{cases} \pi, & r' > 2r - t \\ \arccos \dfrac{t(2r - t) - r'^2}{2(r - t)r'} & r' < 2r - t \end{cases} \tag{16}$$

The two angles α and ϑ are related to each other according to the following equation:

$$r'^2 \sin^2\alpha + (2r - t)r' \sin\alpha \cos\vartheta - t(2r - t) = 0 \tag{17}$$

After some simplifications, one can write the final equation for the potential in acylindrical pore as follows:

$$u(t, r) = \frac{2}{\pi} \int_t^\infty t' \left(\int_0^\vartheta \cos\alpha\, d\vartheta \right) \frac{d^2 u(t', \infty)}{dt'^2}\, dt' \tag{18}$$

The above equation transforms the potential near the flat surface

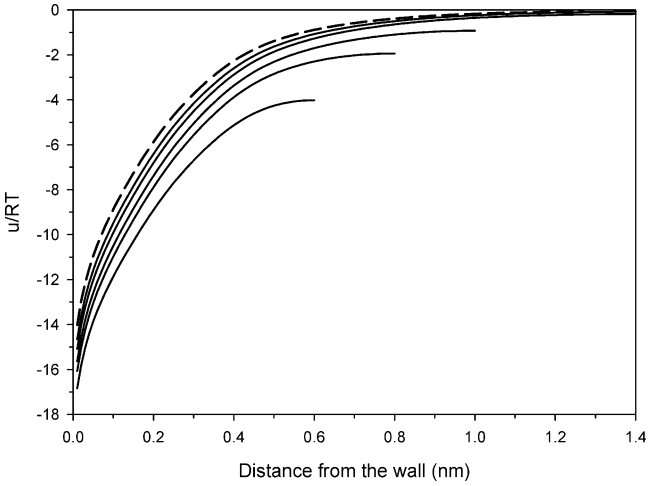

Figure 2. Dependence of the potential inside the cylindrical pore on the distance from the pore wall along the normal to its surface. Solid lines are plotted for the following pore diameters (nm) from the bottom to the top: 1.2, 1.6, 2, 3, and 5. Dashed line corresponds to the flat surface (the pore diameter is infinity).

to the potential inside the cylindrical pore. Thereby, this prescription allows us to circumvent any specification on the solid−fluid interaction at the microscopical level. Figure 2 shows the dependence of the potential in the cylindrical pore on the distance from the surface. Different curves calculated by eq 18 correspond to different pore radii. The dashed line is the potential for a flat surface, which is, in fact, used in the original BdB theory. Comparing the potential for cylinders and that for the flat surface, we see that the enhancement is significant in cylindrical pores, especially smaller pores. This is attributed to the large curvature in those pores. It is seen from the figure that the effect of the pore curvature on the potential is not negligible even when the diameter is as large as 5 nm. It is observed in the figure that the potential tends toward negative infinity as the film thickness approaches zero. It is physically incorrect to have such an extremely large negative number, and it is simply due to the assumptions in the BdB theory. In the framework of BdB theory, the adsorbed film maintains the properties of a macroscopic liquid (i.e., the same density and surface tension as those of liquid) even when its thickness approaches zero. Physically, the dense liquid film loses its integrity at low pressures, at which the adsorbed phase is in a two-dimensional gaslike state. The BdB approach neglects the contribution from the gaslike fluid, which artificially leads to a sharp decrease in the solid−fluid potential. This problem can be resolved by considering the adsorbed phase as an equilibrium system involving the liquid film and the vapor as coexisting phases, both of which constitute the adsorbed phase, rather than just the liquid film. At high pressures, the contribution of the vaporlike part to the amount adsorbed is negligibly small, and the original version of the BdB theory is numerically correct. At extremely small pressures, however, the adsorbed phase is gaslike, and any further decrease of the amount adsorbed with pressure would not result in a decrease of the solid−fluid potential. In other words, the liquidlike adsorbed film appears only at a critical value of the bulk pressure as a result of condensation of the vaporlike adsorbed fluid. Once it appears, the liquid film already has nonzero thickness, which, to some extent, justifies the ascription macroscopic properties to this filmlike density and the surface tension. Such details may be introduced in the model, but it would not appreciably affect the results of its application to mesoporous systems.

2.1.4. Equilibrium Evaporation in the Cylindrical Pore. According to the classical representation, the evaporation occurs via the receding of the semispherical menisci from the open pore ends until complete emptying of the inner core, which occurs at the equilibrium transition pressure. The equilibrium transition occurs at a constant value of the thermodynamic potential. Hence, the thermodynamic potential Ω_f for the completely filled pore must be equal to the potential Ω_e for the emptied core at the same evaporation pressure p_{ev}. Explicit expressions for both values may be obtained from the same eq 9 accounting for the fact that in the case of cylindrical geometry $S = 2\pi(r - t')L$ in the integrand, $S_c = 2\pi rL$, and $S_t = 2\pi(r - t)L$, where L is the length of the pore. Then, one can write the following equations for the thermodynamic potentials:

$$\frac{\Omega_f}{\pi L \rho_L} = -r^2 RT \ln(p_{ev}/p_0) + 2\gamma_c \upsilon_M r + 2\int_0^r (r - t')u(t', r)\,dt'$$

$$\frac{\Omega_e}{\pi L \rho_L} = -t(2r - t)RT \ln(p_{ev}/p_0) + 2\gamma_c \upsilon_M r + 2\gamma \upsilon_M (r - t) + 2\int_0^t (r - t')u(t', r)\,dt' \quad (19)$$

The equalization of the RHSs of the above equations gives the following condition:

$$RT \ln(p_{ev}/p_0) = -\frac{2\gamma \upsilon_M}{(r - t)} + \frac{2}{(r - t)^2}\int_t^r (r - t')u(t', r)\,dt' \quad (20)$$

This equation resembles the Kelvin equation for the semispherical meniscus but additionally includes the potential average over the adsorbed film volume in its RHS.

Once the evaporation has completed, the thickness of the liquid film adsorbed on the pore wall must correspond to the minimum of the grand thermodynamic potential, which is expressed in eq 10. Substitution of the area of the liquid−vapor interface $S_t = 2\pi(r - t)L$ into eq 10 leads to the following result:

$$RT \ln(p/p_0) = -\frac{\gamma \upsilon_M}{(r - t)} + u(t, r) \quad (21)$$

The Cohan equation[7] commonly used in the literature is similar to the above equation when the solid−fluid potential is set to zero. This suggests that the Cohan equation is valid in the region of the pore where solid−fluid potential is negligible (i.e., very large pores). At the transition point, eqs 20 and 21 are simultaneously satisfied. Combining those equations leads to the final equation for the equilibrium transition (capillary evaporation):

$$\frac{2}{(r - t)^2}\int_t^r (r - t')u(t', r)\,dt' - u(t, r) - \frac{\gamma \upsilon_M}{(r - t)} = 0 \quad (22)$$

Given a pore radius r, this equation gives the root $t = t_{ev}$ (subscript ev is for evaporation) for the statistical film thickness and then the potential $u(t_{ev}, r)$. Substitution of these values into eq 20 will yield the relative pressure p_{ev}/p_0 for capillary evaporation.

2.1.5. Spinodal Condensation in the Cylindrical Pore. During adsorption, the cylindrical meniscus is formed. Adsorption equilibrium corresponds to the minimum of the thermodynamic grand potential. This has been described in eq 21. For the

solution of this equation to be a local minimum, the second derivative of the grand potential with respect to the amount adsorbed n must be positive. For adsorbed film thickening to occur, this second derivative must be positive. As the pressure increases, this second derivative decreases, and when the pressure approaches a critical value p_{cond} (vaporlike spinodal point), it becomes zero. At this instant, the system loses its mechanical stability, and the global minimum of the thermodynamic grand potential is simply the one corresponding to the complete filling of the cylindrical pore. This is the phenomenon of capillary condensation. Because in this spinodal point, the first and the second derivatives of Ω with respect to n are both zero, it is equivalent to the requirement that the second derivative of Ω with respect to the adsorbed film thickness t is also zero. Mathematically, the condition of the spontaneous pore filling may be expressed as follows:

$$\frac{\partial^2}{\partial t^2}\left(\frac{\Omega}{2\pi\rho_L L}\right) = RT\ln(p/p_0) - u(t, r) + (r - t)\frac{\mathrm{d}u(t, r)}{\mathrm{d}t} = 0 \tag{23}$$

Combining this equation with eq 20 will lead to the following condition of stability loss:

$$\frac{\mathrm{d}u(t, r)}{\mathrm{d}t} - \frac{\gamma v_M}{(r - t)^2} = 0 \tag{24}$$

For a given pore of radius r, we can solve the above equation for the upper limit of the thickness t_{cond} of the adsorbed film, which remains stable. The pressure corresponding to this limit of film thickness, p_{cond}, can be obtained from eq 20.

2.1.6. Local Isotherms in the CDP−BdB Theory. Having obtained the upper limit of the adsorbed film thickness for a pore of radius r, we can now determine the local adsorption isotherm. The maximum amount that can be accommodated inside a pore is the volume of the liquid that is needed to fill that pore. The local isotherm can be expressed as the fraction of that maximum capacity versus pressure. Thus, for a pore of radius r, the pore will be either layered with adsorbed film or completely filled with liquid. The former is when the pressure is less than p_{cond}, while the latter is the case when $p > p_{cond}$. Therefore, the local isotherm can be expressed mathematically as

$$\theta = \frac{t}{r}\left(2 - \frac{t}{r}\right) \qquad \text{for } p < p_{cond} \tag{25}$$

and it is equal to unity when p is greater than p_{cond}.

2.2. Density Functional Theory in the Case of Amorphous Solids. The background of the DFT is widely represented in the literature.[4,45−48] Here, we follow Tarazona's version of nonlocal DFT based on the smoothed density approximation (SDA).[4,45,49] In the case of an open system (grand canonical ensemble), the density distribution in a confined pore volume is determined for the minimum of the grand thermodynamic potential defined as follows:

$$\Omega = \int \rho(\mathbf{r})\{ f_{id}(\mathbf{r}) + f_{ex}[\bar{\rho}(\mathbf{r})] + u^{int}(\mathbf{r}) + u^{ext}(\mathbf{r}) - \mu\}\, \mathrm{d}\mathbf{r} \tag{26}$$

Here, ρ is the local density of the adsorbed fluid; μ is the chemical potential, which is specified for each equilibrium point; f_{id}, f_{ex}, and u^{int} are the ideal, excess (repulsive), and attractive components of the intrinsic Helmholtz free energy of the adsorbed phase, respectively; u^{ext} is the external component of the Helmholtz free energy associated with the solid−fluid interaction. The ideal term is given by

$$f_{id}(\mathbf{r}) = k_B T\{\ln[\Lambda^3\rho(\mathbf{r})] - 1\} \tag{27}$$

where Λ is the thermal de Broglie wavelength and k_B is Boltzmann's constant.

2.2.1. Modeling of Fluid−Fluid and Solid−Fluid Repulsive Potentials. The excess Helmholtz free energy is defined by the Carnahan−Starling (CS) equation for the equivalent gas of hard spheres,[50] which can be represented as a function of the void volume as follows

$$f_{ex}(\bar{\rho}) = k_B T\frac{1 + 2\bar{v} - 3\bar{v}^2}{\bar{v}^2} \qquad \bar{v} = 1 - \bar{\rho}/\rho_m \tag{28}$$

where $\rho_m = 6/(\pi d_{HS}^3)$ is the maximal fluid density possible and d_{HS} is the equivalent hard sphere diameter. The void volume v is the fraction of volume not occupied by the equivalent hard spheres, which can be interpreted as the volume fraction accessible to fluid molecules. The reason to operate this variable instead of the density is that inaccessible volume in the vicinity of a given point may be due to the presence of surrounding fluid molecules as well as the hard solid wall. Hence, the void volume is more general characteristic compared to the fluid density, which uniquely defines the excess free energy associated with repulsive forces: the less the void volume, the larger the repulsive forces.

According to the Tarasona SDA, the smoothed density $\bar{\rho}$ may be expressed by the following power series:

$$\bar{\rho}(\mathbf{r}) = \bar{\rho}_0(\mathbf{r}) + \bar{\rho}_1(\mathbf{r})\bar{\rho}(\mathbf{r}) + \bar{\rho}_2(\mathbf{r})[\bar{\rho}(\mathbf{r})]^2 \tag{29}$$

with

$$\bar{\rho}_i(\mathbf{r}) = \int \rho(\mathbf{r}')\omega_i(|\mathbf{r} - \mathbf{r}'|)\, \mathrm{d}\mathbf{r}' \qquad i = 0, 1, 2 \tag{30}$$

The weight functions $\omega_0(r)$, $\omega_1(r)$, and $\omega_2(r)$ are defined in the region of two fluid−fluid collision diameters σ_{ff}.[45] In terms of the void volume, the above equations may be easily rewritten as follows:

$$\bar{v}(\mathbf{r}) = \bar{v}_0(\mathbf{r}) + \rho_m\bar{v}_1(\mathbf{r})[1 - \bar{v}(\mathbf{r})] + \rho_m^2\bar{v}_2(\mathbf{r})[1 - \bar{v}(\mathbf{r})]^2 \tag{31}$$

where

$$\bar{v}_i(\mathbf{r}) = \int v(\mathbf{r}')\omega_i(|\mathbf{r} - \mathbf{r}'|)\, \mathrm{d}\mathbf{r}' \qquad i = 0, 1, 2 \tag{32}$$

Here, $v(\mathbf{r})$ is the local value of void volume (i.e., $v(\mathbf{r}) = 1 - \rho(\mathbf{r})/\rho_m$). It is important to note that in the proximity of the pore wall the integral in the above equation is taken over the volume that does not include the pore wall volume. It means that the void volume is zero inside the solid constituting the pore wall, which is simply equivalent to the statement that the volume occupied by the solid is not accessible to the fluid molecules. This self-evident condition is not realized in conventional applications of NLDFT to adsorption systems. In the proximity of the solid−fluid interface, the integrand in eq 30 is implied to be zero in the volume occupied by the solid, which means that the void volume is maximal ($v = 1$) in that region. In other words, in conventional applications of the NLDFT, the smooth void volume is overestimated in the proximity of the pore wall resulting in the underestimation of the excess Helmholtz free energy (i.e., the contribution of the solid surface to repulsive forces is not accounted for). This shortcoming is compensated

by the explicit accounting for the repulsive forces in the LJ solid−fluid potential. This is reasonable in the case of crystalline structures such as graphitized carbon black, because the nearly two-dimensional fluid molecular layer closest to the solid surface is at a distance of about one solid−fluid collision diameter from the surface. At this distance, the contribution of the solid to the excess free energy is negligibly small in the framework of the CS equation. However, this contribution becomes substantial in the case of amorphous solids. It is known from the literature that the conventional NLDFT always fails to quantitatively correlate the adsorption isotherms on disordered materials such as silica, leading to artificial layering not observed experimentally. The deviation between experimental and theoretical isotherms is usually ascribed to the surface energetic heterogeneity; yet, the more important factor seems to come from the implicit replacement of the disordered structure by the perfect crystalline structure of the solid. In this case, the sharp solid−fluid potential minimum will form the 2D molecular layer of the fluid, which, in its turn, causes the highly layered adsorbed fluid structure.

2.2.2. Modeling of Attractive Potentials for Fluid−Fluid and Solid−Fluid Interaction. The attractive part of the Helmholtz free energy in the NLDFT is modeled in the framework of the mean field approximation

$$u^{\text{int}}(\mathbf{r}) = \frac{1}{2}\int \rho(\mathbf{r}')\phi_{\text{ff}}(|\mathbf{r}-\mathbf{r}'|)\,\mathrm{d}\mathbf{r}' \tag{33}$$

where the fluid−fluid attractive pair potential ϕ_{ff} is defined by the Weeks−Chandler−Andersen (WCA) perturbation scheme:[51]

$$\phi_{\text{ff}}(r) = \begin{cases} -\epsilon_{\text{ff}}, & r < r_{\text{m}} \\ 4\epsilon_{\text{ff}}[(\sigma_{\text{ff}}/r)^{12} - (\sigma_{\text{ff}}/r)^{6}], & r_{\text{m}} < r < r_{\text{c}} \\ 0, & r > r_{\text{c}} \end{cases} \tag{34}$$

Here, r and r_{c} are the distances between the molecules and the cutoff distance, respectively, ϵ_{ff} is the potential well depth, σ_{ff} is the fluid−fluid collision diameter, $r_{\text{m}} = 2^{1/6}\sigma_{\text{ff}}$ is the distance at which the potential is minimum. The WCA potential is, in fact, the LJ pair potential with a subtracted repulsive term.

In the present paper, we use the analogous WCA scheme to account for the solid−fluid interaction. It is justified by the fact that the repulsive component of the solid−fluid interaction has already been accounted for with the CS equation for the excess free energy, so there is no need to account for this one more time by the repulsive term of the LJ pair potential. At the same time, we find it reasonable to distinguish in the general case the attractive potential between a fluid molecule and solid surface atoms from that between the molecule and the rest of the solid. For example, the silica surface may contain a different amount of silanols (i.e., hydroxyl groups) or may be modified by octyldimethylsilyl ligands,[52] which substantially changes the adsorption properties of siliceous materials. In this general case, the solid−fluid attractive potential can be written as follows:

$$u^{\text{ext}}(\mathbf{r}) = \int_V \phi_{\text{sf}}^{(\text{V})}(|\mathbf{r}-\mathbf{r}'|)\rho_{\text{s}}^{(\text{V})}\,\mathrm{d}\mathbf{r}' + \int_S \phi_{\text{sf}}^{(\text{S})}(|\mathbf{r}-\mathbf{r}'|)\rho_{\text{s}}^{(\text{S})}\,\mathrm{d}\mathbf{r}' \tag{35}$$

where

$$\phi_{\text{sf}}^{(l)}(r) = \begin{cases} -\epsilon_{\text{sf}}^{(l)} & r < r_{\text{m}}^{(\text{s})} \\ 4\epsilon_{\text{sf}}^{(l)}[(\sigma_{\text{sf}}/r)^{12} - (\sigma_{\text{sf}}/r)^{6}] & r_{\text{m}}^{(\text{s})} < r < r_{\text{c}}^{(\text{s})} \\ 0, & r > r_{\text{c}}^{(\text{s})} \end{cases} \tag{36}$$

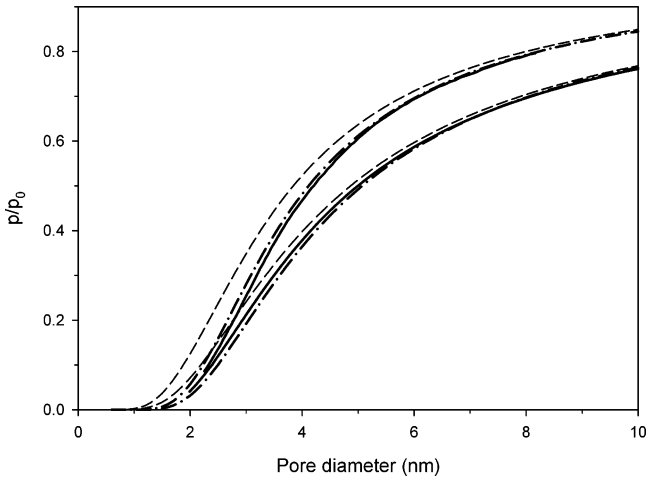

Figure 3. Evaporation and condensation pressure dependence on the pore diameter for the system N_2−siliceous cylindrical pore at 77.35 K predicted by the NLDFT (solid lines), the modified BdB theory (dash−dotted lines), and the original BdB theory (dashed lines). The lower curves are for evaporation, and the upper curves are for the condensation.

TABLE 1: Molecular Parameters for the System N_2−Silica at 77 K

fluid−fluid			solid−fluid		
σ_{ff} (nm)	d_{HS} (nm)	$\epsilon_{\text{ff}}/k_{\text{B}}$ (K)	σ_{sf} (nm)	$\rho_{\text{s}}^{(\text{V})}\epsilon_{\text{sf}}^{(\text{V})}/k_{\text{B}}$ (K nm^{-3})	$\rho_{\text{s}}^{(\text{S})}\epsilon_{\text{sf}}^{(\text{S})}/k_{\text{B}}$ (K nm^{-2})
0.3575	0.3575	94.45	0.2988	6406	640.2

Here, V and S are the volume and the surface area of the solid, respectively, $\rho_{\text{s}}^{(\text{V})}$ is the number density of the solid, $\rho_{\text{s}}^{(\text{S})}$ is the density of solid atoms on the surface, ϵ_{sf} and σ_{sf} are the solid−fluid potential well depth and the solid−fluid collision diameter, respectively; l = V for volume atoms and l = S for surface solid atoms; $r_{\text{c}}^{(\text{s})}$ is the cutoff distance. The multiplier $^1/_2$ at the integral in the RHS of eq 35 is dropped, as all interaction potential is referred to the fluid.

The fluid−fluid molecular parameters ϵ_{ff}, σ_{ff}, and d_{HS} are determined from the bulk phase properties (i.e., the saturation pressure, the density of liquid at this pressure, and the surface tension). The solid−fluid parameters have been determined by the least-squares procedure. The parameters for the system nitrogen−silica at 77.3 K are presented in Table 1.

The fluid−fluid parameters were taken from ref 53. The cutoff distance is $5\sigma_{\text{ff}}$ for fluid−fluid interaction and $4.4\sigma_{\text{sf}}$ for fluid−solid interaction. The correlative ability of the improved NLDFT is demonstrated in Figure 1 for the nitrogen adsorption isotherm on nonporous silica LiChrospher Si-1000. The dashed line plotted with the NLDFT completely merges with the thin solid line, which is the fitting curve. The dash−dotted line is plotted with the conventional NLDFT using the 10-4 LJ potential for the solid−fluid interaction for the parameters reported in ref 53. As is seen from the figure, the conventional NLDFT correlates the experimental isotherm very poorly and leads to the pronounced molecular layering for the reasons discussed above. At the same time, the improved approach adapted to adsorption on amorphous solids demonstrates excellent results, which are most probably the evidence of its adequacy to the system of fluid−amorphous solid.

3. Results

Theoretical dependencies of capillary condensation and capillary evaporation pressures on the pore diameter are

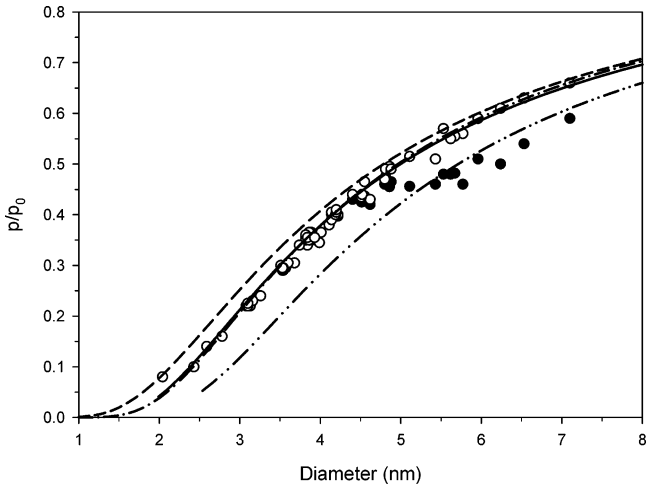

Figure 4. Comparison of the theoretical equilibrium transition pressure−diameter dependence against experimental data on N_2 adsorption at 77.3 K in a series of MCM-41 samples.[24] Open symbols are for condensation, and filled symbols are for evaporation. Solid line is plotted with the improved NLDFT at the solid−fluid molecular parameters determined from the N_2 adsorption isotherm on nonporous silica sample LiChrospher Si-1000 for the specific surface area 24 m^2/g. Dash−double dotted line is calculated with the same version of the developed NLDFT with the solid−fluid parameters corresponding to the specific surface area 19.65 m^2/g. It is seen that the decrease of the reference system surface area estimation leads to nearly parallel shift of the computation curve toward the lower pressures making the curve increasingly deviant from the experimental dependence. Dash−dotted line and dashed line are calculated with the modified and original BdB theories, respectively, for the specific surface area 25 m^2/g.

presented in Figure 3 for the developed version of the NLDFT and CDP−BdB theory, and for the original BdB theory. There are three pairs of curves plotted with corresponding theories, with the lower curve of each pair for the evaporation and the upper curve for the condensation. As is seen from the figure, the original BdB theory (dashed lines) overestimates the pressures of evaporation and condensation for sufficiently small pores. This is because the solid−fluid potential of the original BdB is underestimated, because it does not account for the effect of curvature. The CDP−BdB theory leads to the dependencies, which are significantly closer to those obtained with the NLDFT. The only difference is that the width of the hysteresis loop predicted by the CDP−BdB theory is a bit wider than that obtained by the NLDFT, with the medians being nearly coincidental. At the region of pore size larger than 6 nm, the evaporation and condensation pressures predicted by the CDP−BdB theory are completely in agreement with those predicted by the NLDFT, while the agreement between the original BdB theory and the NLDFT is observed only when pore diameter is greater than 10 nm. Note that the NLDFT predicts the critical hysteresis pore diameter of 2 nm, while the BdB theory does not predict the critical diameter at all.

Experimental dependencies of evaporation and condensation pressures on the pore diameter obtained from the experimental data of nitrogen adsorption in MCM-41 samples[24] are presented in Figure 4. The figure shows that the solid line obtained with the improved NLDFT for the equilibrium transition excellently matches the experimental dependency measured for the capillary condensation, suggesting that the adsorption branch of the isotherm is the equilibrium transition. As is known, the classical scenario[54] predicts the capillary condensation at the limiting point of the metastable adsorption branch (the so-called vapor-like spinodal pressure), where the adsorbed liquid film loses its mechanical stability. The capillary evaporation was claimed to occur by the receding of the semispherical menisci from the pore ends at the equilibrium transition pressure. However, there is unambiguous experimental evidence that the adsorption branch of the hysteresis loop is equilibrium, while the desorption branch occurs with the delay.[10,12,30,31,44] To date, such a contradiction has been construed only by invoking additional assumptions such as the pore-blocking effect[37,55,56] and energetic surface heterogeneity.[57] Figure 4 may be considered as additional proof that the adsorption branch of the isotherm is the thermodynamic equilibrium isotherm, but it is worthwhile to note that neither the CDP−BdB theory nor the improved NLDFT invoke the pore wall surface heterogeneity or surface roughness; however, they perfectly match the experimental data. An explanation for this is as follows: The solid−fluid molecular parameters determined from the reference adsorption isotherm of a flat surface depend on the specific surface area, and very often, this value is taken to be the one obtained from the Brunauer−Emmett−Teller (BET) method. However, as was mentioned above, this approach is quite unreliable and leads to different values of the BET surface area depending on the pressure range used in the linear plot.[43] For this reason, we varied the specific surface area of the nonporous silica sample in the region of its uncertainty. Each time, we evaluated the solid−fluid molecular parameters corresponding to the best fit of the experimental *t*-curve, which were further used for NLDFT prediction of the condensation/evaporation pressure versus the pore diameter. Our goal was to find the set of molecular parameters that simultaneously ensure reasonable correlation of the experimental condensation pressure by the spinodal condensation curve and the experimental evaporation pressure by the equilibrium transition curve. However, in all cases, the steepness of the predicted spinodal condensation pressure−diameter dependence was markedly larger than that of the experimental dependence. In regard to the equilibrium transition pressure−diameter curve, the variation of the reference surface area resulted in a vertical shift of the curve. As an example, we present in Figure 4 the equilibrium transition curve (dash−dotted line) plotted for the specific surface area of 19.65 m^2/g, which was used to construct the *t*-curve. This curve is quite close to the experimental evaporation pressure for diameters larger than 5.5 nm, but by no means is suitable at lower pressures, where the isotherm shows reversibility and, hence, must correspond to the true equilibrium. The striking result is that there is only the possibility to superimpose the predicted equilibrium transition curve onto the experimental condensation pressure−diameter curve, as has been done in the figure with the specific surface area of the reference silica of 24 m^2/g. It is worthwhile to note that by using the commonly used projection area of the nitrogen molecule of 0.162 nm^2 the conventional BET method that was applied on data points in the reduced pressure range of 0.06 to 0.2 gives a surface area of 27.2 m^2/g. If the projection area was taken to be 0.135 nm^2, as was recommended by Jelinek and Kovats,[58] the specific surface area of the reference silica is 22.6 m^2/g. The surface area of 24 m^2/g obtained by our procedure falls between these two values, and therefore, it provides a realistic estimate of the reference silica surface area. The result that the condensation pressure−diameter dependence can be accurately described by the theoretical dependence for the equilibrium transition pressure is quite obscure, and requires further investigation in this area. However, at the present stage, one can use the above observation for pore size distribution analysis in a formal way.

Despite the good agreement between NLDFT and the CDP−BdB theory demonstrated in Figure 3, it is worth noting that

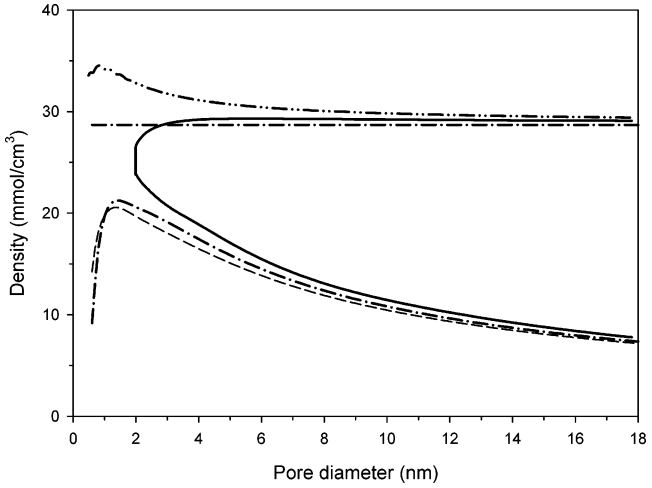

Figure 5. Average nitrogen density in the cylindrical pore at the equilibrium transition pressure and at the saturation pressure. The upper and lower branches of solid curve are calculated by the NLDFT and correspond to the onset and the completion of pore emptying at the equilibrium transition pressure, respectively. The same branches predicted by the modified BdB theory are plotted by dash−dotted line, with the density for the upper branch being the liquid-phase density. Dashed line is plotted with the original BdB theory. The dash−double dotted line shows the adsorbed nitrogen density predicted by the NLDFT at the saturation pressure.

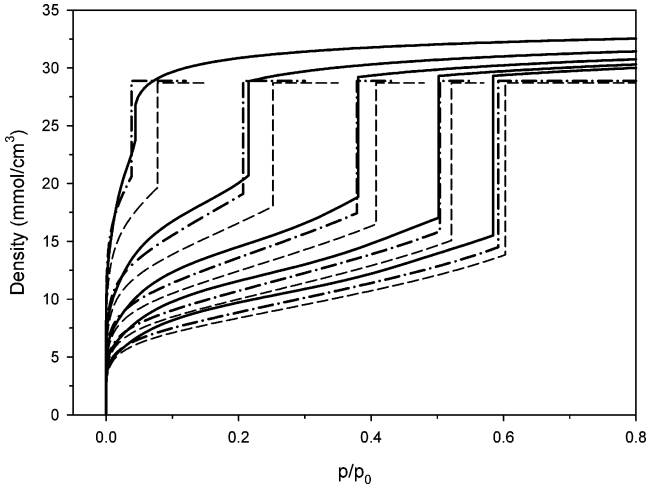

Figure 6. Local nitrogen adsorption isotherms for cylindrical silica pores generated by the improved NLDFT (solid lines), the modified BdB theory (dash−dotted lines), and the original BdB theory (thin dashed lines). The prediameter from left to right (nm): 2, 3, 4, 5, and 6.

the PSD analysis is highly susceptible to even small deviations in the filling pressure. For this reason, it seems to be more logical to adjust the surface area of the reference silica by means of the same theory that is used for the analysis of porous siliceous materials. This means that when we use the BdB theory it is not necessary to resort to the surface area of the reference system determined by the NLDFT, while it could be done by the BdB itself. In doing so, we found that perfect fitting of experimental condensation pressures by the BdB curve (dash−dotted curve in Figure 4) corresponds to the specific surface area of the nonporous LiChrospher silica of 25 m^2/g. This value is 4% larger than that determined by the NLDFT, which seems to be reasonable, as the BdB theory does not account for the compression of the adsorbed phase. Therefore, the same amount adsorbed having the density of the saturation liquid can be accommodated by a larger surface compared to the case of the compressed liquid. This shortcoming is inherent in all continuum approaches and apparently should be eliminated in their further development. At present, the small tuning of the reference specific surface area that we used resulted in the perfect agreement of the filling pressure curves obtained with the molecular and continuum approaches, while the original BdB theory substantially overpredicts the experimental condensation pressure at diameters smaller than about 6 nm.

Figure 5 shows the effect of the pore size on the nitrogen density averaged over the pore cross-section at the instant before the capillary evaporation (upper solid and dash−dotted lines) and after the evaporation has occurred (lower curves). These upper and lower curves join at the point exactly corresponding to 2 nm, which is the critical size of the capillary condensation predicted by the NLDFT. The average nitrogen density in the completely filled pore before the instant of capillary evaporation is close to the liquid density. The dash−dotted line is the average density calculated by the NLDFT at the saturated vapor pressure. As can be seen from the figure, the density of adsorbed nitrogen at this pressure substantially exceeds that of the bulk liquid. This is due to the compressibility of condensed fluid at high pressure inside the pore. This feature is built into the NLDFT, but is not accounted for in the BdB theory. For this reason, the average nitrogen density in the completely filled pore predicted in the BdB theory is always the same as that of the liquid nitrogen. The lower branch of the density−diameter dependency predicted by the BdB theory is in reasonably good agreement with the NLDFT prediction, but the CDP−BdB version leads to a slightly better agreement compared to that for the original BdB theory. In any case, as can be seen from the figure, 2 nm is the lower limit of the applicability of the continual BdB approach. It should be noted that the compressibility of the liquidlike fluid predicted by DFT is substantially larger than the experimental compressibility, and so, the actual adsorbed phase density in the filled pore does not deviate from the liquid density as significantly as is shown in the figure. However, it again indicates that the compressibility should be incorporated into the BdB theory in its further modification.

It is more informative for us to compare the local isotherms in pores of different sizes, ranging from 2 to 6 nm, and this is shown in Figure 6. The isotherms obtained by the CDP−BdB approach agree with those from the NLDFT reasonably well for all pore diameters, while the original BdB theory substantially underestimates the density in the region of polymolecular adsorption on the pore walls and predicts a higher transition pressure, especially for small pore sizes. We used the set of such isotherms for the pore size distribution analysis.

3.1. Pore Size Distribution Analysis of MCM-41 Silica Samples. The comparison of the molecular approach (NLDFT) with the two versions of the continuum approach (BdB theory) has been done using nitrogen adsorption isotherms at 77 K on a series of six MCM-41 samples having pores from 3 to about 5 nm[59] and three MCM-41 samples with larger pores ranging from 5.5 to 6.5 nm.[10]

Given the local isotherm at pressure p and pore diameter D, the overall isotherm can be expressed as the following integral:

$$a = \int_{D_{\min}}^{D_{\max}} f(D)\rho(D, p/p_0)\, \mathrm{d}D \qquad (37)$$

Here, $f(D)$ is the distribution function of pore volume over pore diameter, and $\rho(D, p/p_0)$ is the local isotherm. The boundaries $D_{\min}$ and $D_{\max}$ were chosen as 0.6 and 16 nm, respectively. We used the Tikhonov regularization method[60,61] with the combination of nonnegative least-squares fitting in the form presented

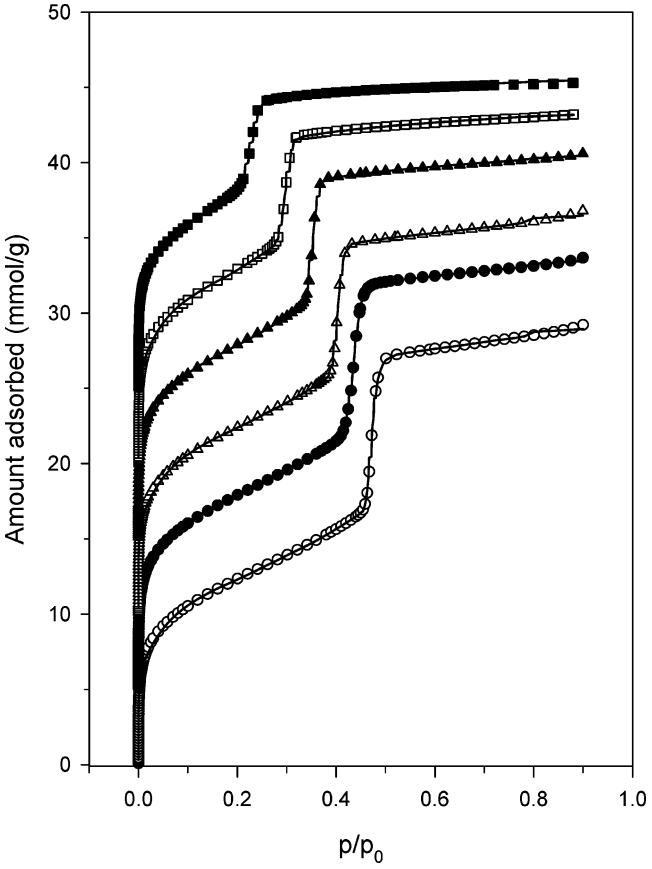

Figure 7. Nitrogen adsorption isotherms for MCM-41 silica samples at 77.3 K. Number of alkyl groups in the surfactant chain *n* in the designations of samples C_n: ○, 22; ●, 20; △, 18; ▲, 16; □, 14; ■, 12. Amounts adsorbed for C_{20}, C_{18}, C_{16}, C_{14}, and C_{12} are incremented by 5, 10, 15, 20, and 25 mmol/g, respectively.

elsewhere.[62] The local isotherm was determined as described in the previous sections.

The adsorption branches of isotherms for the first series are presented in Figure 7. In all isotherms, the steep rise of the amount adsorbed is observed in the narrow pressure range corresponding to the phase transition, which indicates the high degree of geometrical homogeneity of these samples. Solid lines are the fitted curves obtained with the NLDFT. As can be seen from the figure, the fitting of the experimental data is perfect, which is a necessary (but not sufficient) condition to obtain a reliable pore size distribution. Similar perfect fitting is also achieved with the BdB approaches. Interestingly, up to this time, we faced the situation in which only the molecular approaches such as DFT and GCMC, being the most sophisticated, encountered, however, the greatest problems with the quantitative description of experimental adsorption isotherms. The improved version of the NLDFT as applied to amorphous solids no longer has this problem.

The PSDs for the first series of MCM-41 samples are presented in Figure 8. As was expected, the main peaks in the PSDs obtained with the NLDFT are very narrow. The CDP−BdB approach produces very similar PSD functions, while the original BdB theory noticeably underestimates pore sizes. The results of PSD analysis are summarized in Table 2.

The asterisk following the abbreviation BdB in Table 2 denotes the modified BdB theory (i.e., the CDP−BdB theory). The pore diameter was determined from the PSD function for the maximum of the main peak. The table shows that the diameters determined with the NLDFT and CDP−BdB theory

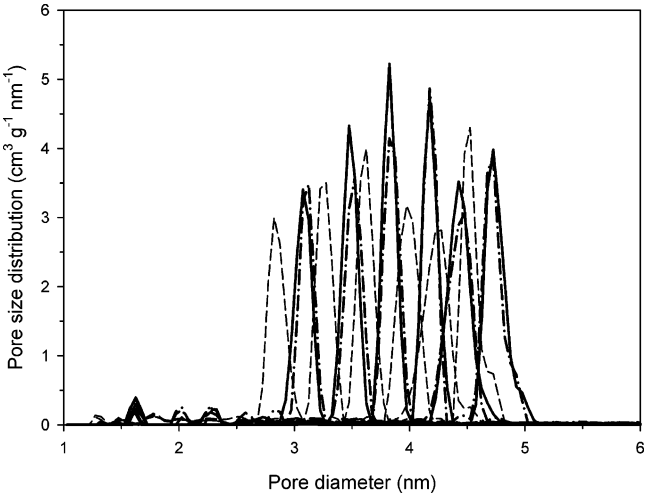

Figure 8. Pore size distributions of MCM-41 samples determined from nitrogen adsorption isotherms at 77.3 K with the proposed version of NLDFT (solid lines), with the original BdB theory (thin dashed lines), and with the modified BdB theory (dash−dotted lines). PSD curves correspond to samples (from left to right): C_{12}, C_{14}, C_{16}, C_{18}, C_{20}, and C_{22}.

TABLE 2: Structural Properties of MCM-41 Samples

sample	D_{XRD} (nm)	pore diameter (nm)			surface area (m^2/g)			pore volume (cm^3/g)		
		NLDFT	BdB*	BdB	NLDFT	BdB*	BdB	NLDFT	BdB*	BdB
C_{12}	3.16	3.08	3.12	2.83	868.1	899.4	1016.9	0.648	0.702	0.706
C_{14}	3.51	3.48	3.52	3.26	875.8	908.5	1012.6	0.741	0.801	0.805
C_{16}	3.87	3.82	3.83	3.61	884.8	920.3	1019.7	0.818	0.879	0.884
C_{18}	4.14	4.17	4.18	3.98	856.6	889.0	979.7	0.856	0.914	0.920
C_{20}	4.51	4.43	4.45	4.25	896.0	929.4	1028.8	0.923	0.983	0.989
C_{22}	4.80	4.73	4.71	4.51	857.1	889.0	979.6	0.942	0.999	1.005

are in good agreement with each other and with the values determined by X-ray diffractometry , while the original BdB theory underestimates the pore diameter. The latter is the reason for the overestimation of the pore surface area with the original BdB approach by about 15%. The CDP−BdB theory also overestimates the pore surface area, but the difference between this value and that determined by the NLDFT does not exceed 4%. The last three columns show that both the CDP−BdB and the original BdB theories overpredict the pore volume by about 8%. This is because the continuous theories do not account for the compressibility of the adsorbed nitrogen.

The nitrogen adsorption isotherms for the second series of large-pore MCM-41 samples are presented in Figure 9. As in the case of the first series, the solid lines are plotted with the modified version of NLDFT. The fitting of the experimental data is again very perfect. The evaluated PSD functions are presented in Figure 10. As can be seen from the figure, in the case of relatively large-pore samples, both versions of the BdB theory lead to similar PSD functions, which are close to that determined with the NLDFT. It shows that the original BdB theory leads to quantitative results if the pore diameter is larger than about 6 nm. The main results obtained with the PSD analysis for these large-pore samples are presented in Table 3.

Because of the broader PSD functions compared to those for the first series, we determined the average pore diameter as the first central moment. One can see from columns 2−5 that the diameters determined with the NLDFT and CDP−BdB approach are in perfect agreement with those determined by the X-ray diffraction technique. The diameters evaluated with the original BdB theory are slightly underestimated but agree reasonablywell with actual pore sizes, because in the case of relatively large pores, the effect of solid surface curvature on the potential is

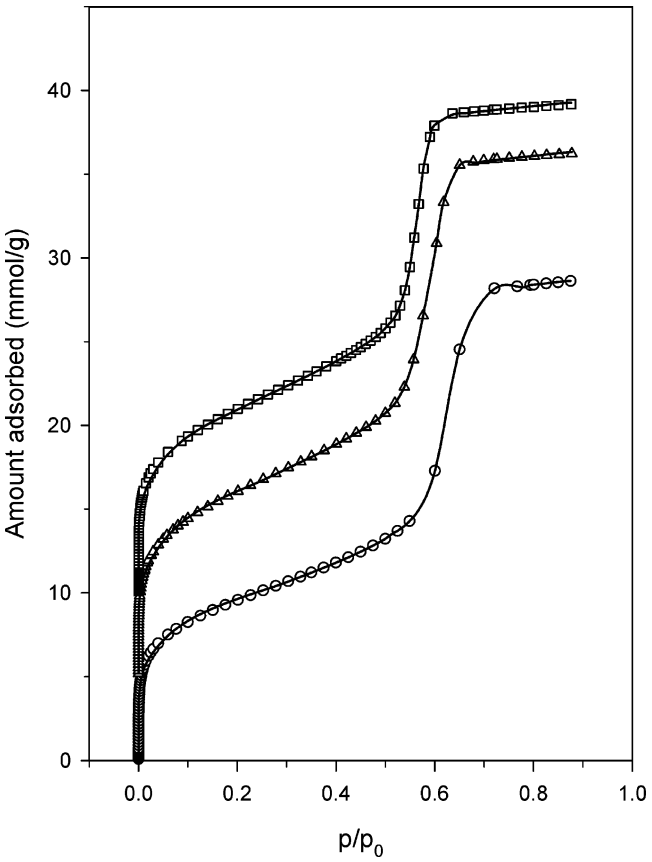

Figure 9. Nitrogen adsorption isotherms for large-pore MCM-41 samples at 77.3 K. The symbols ○, △, and □ correspond to the MCM-41 samples designated in ref 10 as (6.5), (5.5), and (5.0), respectively. Amounts adsorbed for MCM-41 (6.0) and MCM-41 (5.5) are incremented by 5 and 10 mmol/g, respectively.

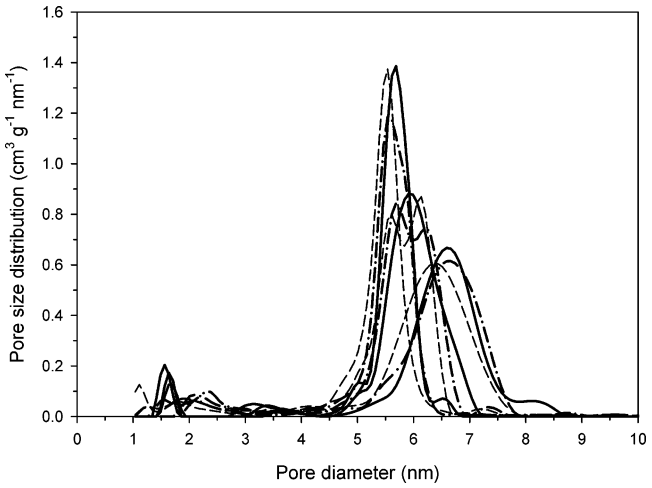

Figure 10. Pore size distributions of large-pore MCM-41 samples determined from nitrogen adsorption isotherms at 77.3 K with the proposed version of NLDFT (solid lines), with the original BdB theory (thin dashed lines), and with the modified BdB theory (dash−dotted lines). PSD curves correspond to samples (from left to right): (5.5), (6.0), and (6.5).

not as significant as in the case of smaller pores. Nevertheless, the surface area of the pores determined with the original BdB theory is substantially larger than that determined with the CDP−BdB theory. This is because of the overlapping of two effects, one of which is the underestimation of the phase transition pressure and the other one is the underestimation of the film thickness for a given pressure. The latter is seen from the local isotherms presented in Figure 6. The last three columns in Table 3 show that both the improved and original BdB theories overestimate the pore volume due to neglecting the adsorbed fluid compressibility.

TABLE 3: Structural Properties of Large-Pore MCM-41 Samples

sample	D_{XRD} (nm)	pore diameter (nm)			surface area (m^2/g)			pore volume (cm^3/g)		
		NLDFT	BdB*	BdB	NLDFT	BdB*	BdB	NLDFT	BdB*	BdB
(5.5)	5.53	5.68	5.62	5.57	757.5	791.1	867.2	0.960	1.011	1.017
(6.0)	5.96	6.01	5.92	5.87	772.6	805.1	877.4	1.031	1.082	1.088
(6.5)	6.53	6.62	6.63	6.43	684.2	691.7	789.8	0.947	0.998	0.997

Our general impression is that mesoporous materials could be effectively characterized not only with the NLDFT but also with the improved BdB theory that incorporates the curvature-dependent adsorption potential. This improved theory, designated as CDP−BdB, maintains the simplicity and self-consistency of the original theory, but has a much larger descriptive capability. It may be further refined by accounting for the adsorbed phase compressibility. These topics will be addressed in our future correspondence.

4. Conclusion

In this paper, the refined Broekhoff and de Boer model incorporating the curvature-dependent adsorption potential (CDP−BdB) has been formulated in a purely continuum macroscopic framework. The comparison of the CDP−BdB approach with the NLDFT adapted to amorphous solid structures has shown that both theories produce very similar pore size distribution functions for the pore sizes larger than 2 nm and therefore may be applicable to the PSD analysis of mesoporous materials. Both theories were tested on the structural analysis of MCM-41 silica samples with pore diameters from 3 to 6.5 nm. It was shown that the pore diameters determined with these theories agree well with those determined by X-ray diffractometry. The renewed BdB theory now can be used as a simple tool for the characterization of mesoporous materials.

Acknowledgment. Support from the Australian Research Council is gratefully acknowledged. M.J. acknowledges the NSF for partial support of this research (grant CHE-0093707).

References and Notes

(1) Zsigmondy, A. *Z. Anorg. Chem.* **1911**, *71*, 356.
(2) Gregg, S. J.; Sing, K. S. W. *Adsorption, Surface Area, and Porosity*; Academic press: London, 1982.
(3) Evans, R.; Marconi, U. M. B.; Tarazona, P. *J. Chem. Phys.* **1986**, *84*, 2376.
(4) Evans, R.; Marconi, U. M. B.; Tarazona, P. *J. Chem. Soc., Faraday Trans.* **1986**, *82*, 1763.
(5) Ruthven, D. M. *Principles of Adsorption and Adsorption Processes*; Wiley: New York, 1984.
(6) Foster, A. G. *Trans. Faraday Soc.*, **1932**, *28*, 645.
(7) Cohan, L. H. *J. Am. Chem. Soc.* **1938**, *60*, 433.
(8) Derjaguin, B. V. *Zh. Fiz. Khim.* **1940**, *40*, 137.
(9) Barret, E. P.; Joyner, L. G.; Halenda, P. P. *J. Am. Chem. Soc.* **1962**, *73*, 373.
(10) Kruk, M.; Jaroniec, M.; Sayari, A. *Langmuir* **1997**, *13*, 6267.
(11) Kruk, M.; Antochshuk, V.; Jaroniec, M.; Sayari, A. *J. Phys. Chem. B* **1999**, *103*, 10670.
(12) Kruk, M.; Jaroniec, M. *Chem. Mater.* **2000**, *12*, 222.
(13) Broekhoff, J. C. P.; de Boer, J. H. *J. Catal.* **1967**, *9*, 8, 15.
(14) Broekhoff, J. C. P.; de Boer, J. H. *J. Catal.* **1968**, *10*, 368, 377, 391.
(15) Lukens, W. W., Jr.; Schmidt-Winkel, P.; Zhao, D.; Feng, J.; Stucky, J. D. *Langmuir* **1999**, *15*, 5403.
(16) Zhu, H. Y.; Lu, G. Q.; Zhao, X. S. *J. Phys. Chem. B* **1998**, *102*, 7371.
(17) Qiao, S. Z.; Bhatia, S. K.; Zhao, X. S. *Microporous Mesoporous-Mater.* **2003**, *65*, 287.

(18) Qiao, S. Z.; Bhatia, S. K.; Nicholson, D. *Langmuir* **2004**, *20*, 389.
(19) Sonwane, C. G.; Bhatia, S. K. *Chem. Eng. Sci.* **1998**, *53*, 3143.
(20) Bhatia, S. K.; Sonwane, C. G. *Langmuir* **1998**, *14*, 1521.
(21) Sonwane, C. G.; Bhatia, S. K. *Langmuir* **1999**, *15*, 5347.
(22) Sonwane, C. G.; Bhatia, S. K.; Calos, N. *Ind. Eng. Chem. Res.* **1998**, *37*, 2271.
(23) Sonwane, C. G.; Bhatia, S. K. *J. Phys. Chem. B* **2000**, *104*, 9099.
(24) Kruk, M.; Jaroniec, M. *Chem. Mater.* **2001**, *13*, 3169.
(25) Inoue, S.; Hanzawa, Y.; Kaneko, K. *Langmuir* **1998**, *14*, 3079.
(26) Kadlec, O.; Dubinin, M. M. *J. Colloid Interface Sci.* **1969**, *31*, 479.
(27) Burgess, C. G. V.; Everett, D. H. *J. Colloid Interface Sci.* **1970**, *33*, 611.
(28) Selvam, P.; Bhatia, S. K.; Sonwane, C. *Ind. Eng. Chem. Res.* **2001**, *40*, 3237.
(29) Groen, J.; Peffer, L. A. A.; Pérez-Ramíres, J. *Microporous Mesoporous Mater.* **2003**, *60*, 1.
(30) Morishige, K.; Ito, M. *J. Chem. Phys.* **2002**, *117*, 8036.
(31) Morishige, K.; Nakamura, Y. *Langmuir* **2004**, *20*, 4503.
(32) Neimark, A. V.; Ravikovitch, P. I. *Microporous Mesoporous Mater.* **2001**, *44*−*45*, 697.
(33) Ravikovitch, P. I.; Wei, D.; Chueh, W. T.; Haller, G. L.; Neimark, A. V. *J. Phys. Chem. B* **1997**, *101*, 3671.
(34) Ravikovitch, P. I.; Neimark, A. V. *Stud. Surf. Sci. Catal.* **2000**, *129*, 597.
(35) Ravikovitch, P. I.; Vishnyakov, A.; Neimark, A. V. *Phys. Rev. E* **2001**, *64*, 011602.
(36) Ravikovitch, P. I.; Neimark, A. V. *Colloids Surf., A* **2001**, *187*−*188*, 11.
(37) Ravikovitch, P. I.; Neimark, A. V. *Langmuir* **2002**, *18*, 9830.
(38) Neimark, A. V.; Ravikovitch, P. I.; Vishnyakov, A. *Phys. Rev. E* **2000**, *62*, 1493.
(39) Gelb, L. D. *Mol. Phys.* **2002**, *100*, 2049.
(40) Vishnyakov, A.; Neimark, A. V. *J. Chem. Phys.* **2003**, *119*, 9755.
(41) Coasne, B.; Pellenq, R. J.-M. *J. Chem. Phys.* **2004**, *120*, 2913.
(42) Cranston, R. W.; Inkley, F. A. *Adv. Catal.* **1957**, *9*, 143.
(43) Jaroniec, M.; Kruk, M.; Olivier, J. P. *Langmuir* **1999**, *15*, 5410.
(44) Kruk, M.; Jaroniec, M. *J. Phys. Chem. B* **2002**, *106*, 4732.
(45) Tarazona, P.; Marconi, U. M. B.; Evans, R. *Mol. Phys.* **1987**, *60*, 573.
(46) Evans, R. In *Fundamentals of Inhomogeneous Fluids*; Henderson, D., Ed.; Marcel Dekker: New York, 1992; Chapter 5.
(47) Lastoskie, C.; Gubbins, K. E.; Quirke, N. *Langmuir* **1993**, *9*, 2693.
(48) Gelb, L. D.; Gubbins, K. E.; Radhakrishnan, R.; Sliwinska-Bartkowiak, M. *Rep. Prog. Phys.* **1999**, *62*, 1573.
(49) Tarazona, P. *Phys. Rev. A* **1985**, *31*, 2672.
(50) Carnahan, N. F.; Starling, K. E. *J. Chem. Phys.* **1969**, *51*, 635.
(51) Weeks, J. D.; Chandler, D.; Andersen, H. C. *J. Chem. Phys.* **1971**, *54*, 5237.
(52) Kruk, M.; Jaroniec, M.; Antochshuk, V.; Sayari, A. *J. Phys. Chem. B* **1999**, *103*, 10670.
(53) Neimark, A. V.; Ravikovitch, P. I.; Grün, M.; Schüth, F.; Unger, K. K. *J. Colloid Interface Sci.* **1998**, *207*, 159.
(54) Everett, D. H. In *The Solid − Gas Interface*; Flood, E. A., Ed.; Marcel Dekker: New York, 1967; Vol. 2, Chapter 36, p 1055.
(55) Matos, J. R.; Mercuri, L. P.; Kruk, M.; Jaroniec, M. *Langmuir* **2002**, *18*, 884.
(56) Kruk, M.; Jaroniec, M.; Sayari, A. *Adsorption* **2000**, *6*, 47.
(57) Maddox, M. W.; Olivier, J. P.; Gubbins, K. E. *Langmuir* **1997**, *13*, 1737.
(58) Jelinek, L.; sz. Kovats, E. *Langmuir* **1994**, *10*, 4225.
(59) Kruk, M.; Jaroniec, M.; Sakamoto, Y.; Terasaki, O.; Ryoo, R.; Ko, Ch. H. *J. Phys. Chem. B* **2000**, *104*, 292.
(60) Tikhonov, A. N. *Dokl. Akad. Nauk SSSR* **1943**, *39*, 195.
(61) Tikhonov, A. N. *Dokl. Akad. Nauk SSSR* **1963**, *153*, 49.
(62) Ustinov, E. A.; Do, D. D. *Langmuir* **2003**, *19*, 8349.